RESEARCH ARTICLE

# Recoding of the Vesicular Stomatitis Virus L Gene by Computer-Aided Design Provides a Live, Attenuated Vaccine Candidate

**Bingyin Wang,[a] Chen Yang,[a] Gergely Tekes,[d] Steffen Mueller,[a,c] Aniko Paul,[a] Sean P. J. Whelan,[b] Eckard Wimmer[a,c]**

Department of Molecular Genetics and Microbiology, Stony Brook University School of Medicine, Stony Brook, New York, USA[a]; Department of Microbiology and Immunobiology, Harvard Medical School, Boston, Massachusetts, USA[b]; Codagenix Inc., Stony Brook, New York, USA[c]; Faculty of Veterinary Medicine, Institute of Virology, Justus-Liebig-University Giessen, Giessen, Germany[d]

**ABSTRACT** **Codon pair bias (CPB), which has been observed in all organisms, is a neglected genomic phenomenon that affects gene expression. CPB results from synonymous codons that are paired more or less frequently in ORFeomes regardless of codon bias. The effect of an individual codon pair change is usually small, but when it is amplified by large-scale genome recoding, strikingly altered biological phenotypes are observed. The utility of codon pair bias in the development of live attenuated vaccines was recently demonstrated by recodings of poliovirus (a positive-strand RNA virus) and influenza virus (a negative-strand segmented RNA virus). Here, the L gene of vesicular stomatitis virus (VSV), a nonsegmented negative-sense RNA virus, was partially recoded based on codon pair bias. Totals of 858 and 623 silent mutations were introduced into a 5′-terminal segment of the viral L gene (designated L1) to create sequences containing either overrepresented or underrepresented codon pairs, designated L1$^{sdmax}$ and L1$^{min}$, respectively. Analysis revealed that recombinant VSV containing the L1$^{min}$ sequence could not be recovered, whereas the virus with the sdmax sequence showed a modest level of attenuation in cell culture. More strikingly, in mice the L1$^{sdmax}$ virus was almost as immunogenic as the parental strain but highly attenuated. Taken together, these results open a new road to attain a balance between VSV virulence and immunogenicity, which could serve as an example for the attenuation of other negative-strand, nonsegmented RNA viruses.**

**IMPORTANCE** **Vesicular stomatitis virus (VSV) is the prototypic rhabdovirus in the order *Mononegavirales*. A wide range of human pathogens belong to this family. Using a unique computer algorithm and large-scale genome synthesis, we attempted to develop a live attenuated vaccine strain for VSV, which could be used as an antigen delivery platform for humans. Recombinant VSVs with distinct codon pair biases were rationally designed, constructed, and analyzed in both cell culture and an animal model. One such recombinant virus, L1$^{sdmax}$, contained extra overrepresented codon pairs in its L gene open reading frame (ORF) and showed promise as an effective vaccine candidate because of a favorable balance between virulence and immunogenicity. Our study not only contributes to the understanding of the underlying mechanism of codon pair bias but also may facilitate the development of live attenuated vaccines for other viruses in the order *Mononegavirales*.**

**Received** 23 February 2015 **Accepted** 27 February 2015 **Published** 31 March 2015

**Citation** Wang B, Yang C, Tekes G, Mueller S, Paul A, Whelan SPJ, Wimmer E. 2015. Recoding of the vesicular stomatitis virus L gene by computer-aided design provides a live, attenuated vaccine candidate. mBio 6(2):e00237-15. doi:10.1128/mBio.00237-15.

**Editor** W. Ian Lipkin, Columbia University



Address correspondence to Eckard Wimmer, eckard.wimmer@stonybrook.edu.

This article is a direct contribution from a Fellow of the American Academy of Microbiology.

Nonsegmented, negative-sense (NNS) RNA viruses include a wide range of established and emerging mammalian pathogens. For most of them, neither vaccines nor antiviral therapeutics with proven efficacy are available (1–3). Vesicular stomatitis virus, an NNS virus of the *Rhabdoviridae*, is an arthropod-borne pathogen that primarily causes acute vesicular disease in livestock (4). However, rare cases of human infection have been reported. Individuals infected with VSV usually develop mild flu-like symptoms, but a single case of encephalitis in a 3-year-old child has been related to VSV infection (5). Nevertheless, VSV serves as an attractive model to study a large number of mammalian pathogens of the *Rhabdoviridae*, including rabies virus (6).

Except for the members of the *Orthomyxoviridae* (e.g., influenza viruses), whose RNA polymerase is a tripartite complex (7), all the negative-strand RNA viruses encode a single large polymerase protein, L, which contains all the enzymatic activities involved in nucleotide polymerization (8) and mRNA modification (9–11). Amino acid sequence comparison of L proteins from multiple NNS viruses revealed six conserved regions (CR I to VI), which led to the notion that the large single L protein might be organized into a series of domains that retain independent catalytic activities (12).

VSV has been used extensively during the last four decades as a laboratory tool to study molecular virology and cell biology. Its relatively innocuous phenotype in human infection makes this virus attractive for clinical application, a potential realized only recently. However, VSV is an infectious agent with neurotoxicity in experimental animals, which poses serious safety concerns for direct human use (13, 14). Here, we report attempts to develop a live attenuated VSV strain, making use of a genetic phenomenon

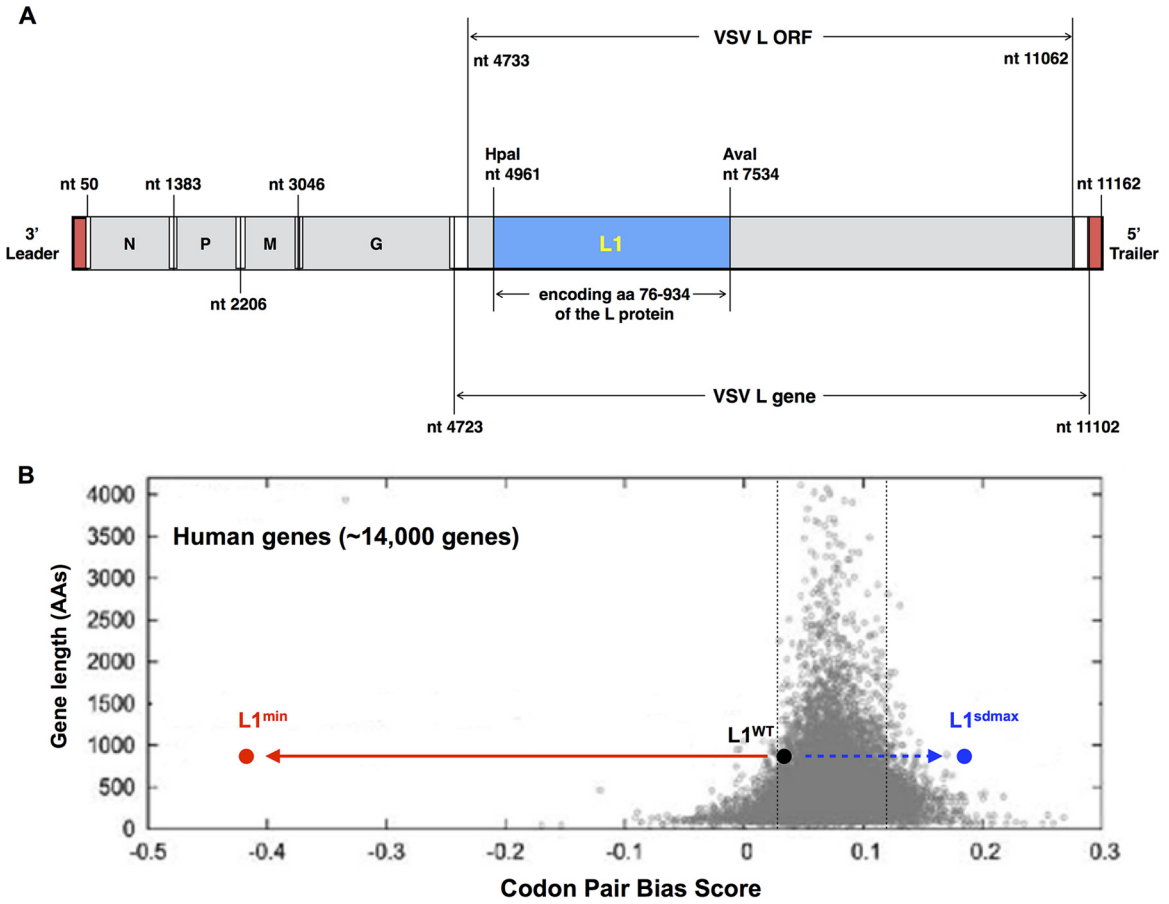


**FIG 1** Genome organization of VSV and construction of L variants. (A) The VSV genome consists of 2 untranslated regions (3′ leader and 5′ trailer; red boxes) and 5 viral genes (N, P, M, G, and L). Like the other four viral genes, the VSV L ORF is flanked by the untranslated regulatory sequences (white boxes) that are essential for transcription initiation and termination. The L1 region (blue box) is between nt 4961 and nt 7534, corresponding to amino acids 76 to 934 of the L protein. $L1^{sdmax}$ and $L1^{min}$ sequences were synthesized *de novo* and incorporated into the parental plasmid pVSV1(+) to replace the WT sequence, using HpaI and AvaI sites. (B) Codon pair bias of human genes and the L1 derivatives plotted against their amino acid lengths.

known as codon pair bias (CPB) (15, 16). CPB, which has been observed in ORFeomes of all organisms studied so far, describes an unexpected irregularity of synonymous codon pairing in genomes of a specific phylum, independent of its genome-wide codon usage. We previously reported that codon pairs are either overrepresented or underrepresented in the genome of a particular organism (17). The nature of a codon pair can be defined by calculating its codon pair bias score (CPS), which is the natural logarithm of the ratio of the observed frequency of the codon pair to the expected frequency. The average of the sum of all CPSs in an ORF indicates the codon pair bias of the entire gene. In our previous experiments involving recoding of viral genomes, we have shown that the viral gene expression can be intentionally altered by a rational design of a coding sequence, based on codon pair bias (17–20). More importantly, the alteration of gene expression is likely a result of the numerous synonymous substitutions, which makes phenotypic reversion nearly impossible (21). This specific property of virus attenuation caused by changing codon pair bias is critical for the development of vaccine strains against RNA viruses, like VSV, described here, whose spontaneous mutation rates are much higher than those of DNA viruses and of other microorganisms (22).

In this study, we examined the impact of recoding the VSV L gene on virus replication in cell culture and on pathogenicity in mice. By using computer-aided design and chemical cDNA synthesis as described before (17, 19, 20), we constructed two recombinant versions of VSV, containing an excess of either underrepresented ("min") or overrepresented ("sdmax") codon pairs. Because of the large size of the L ORF, we focused on the N-terminal segment of the L gene, designating the recoded segments $L1^{min}$ and $L1^{sdmax}$. The $L1^{min}$ design led to a nonviable virus, probably because of poor expression of the L gene. Surprisingly, the $L1^{sdmax}$ design caused modest attenuation in cell culture, whereas this variant was highly attenuated in the mouse model. Moreover, the $L1^{sdmax}$ virus exhibited potent immunogenicity that fully protected vaccinated mice from lethal challenge with wild-type (WT) VSV. These observations suggest that the $L1^{sdmax}$ virus could be developed into a promising vaccine candidate or a vector for the delivery of immunologically important antigens.

## RESULTS

**Construction and characterization of L recoded VSV variants in tissue culture.** We recoded a large N-terminal segment of the L gene ORF, L1, by computer algorithm-aided design (Fig. 1A). Without alteration of codon usage or amino acid sequence, we rearranged the positions of existing codons to generate either un-

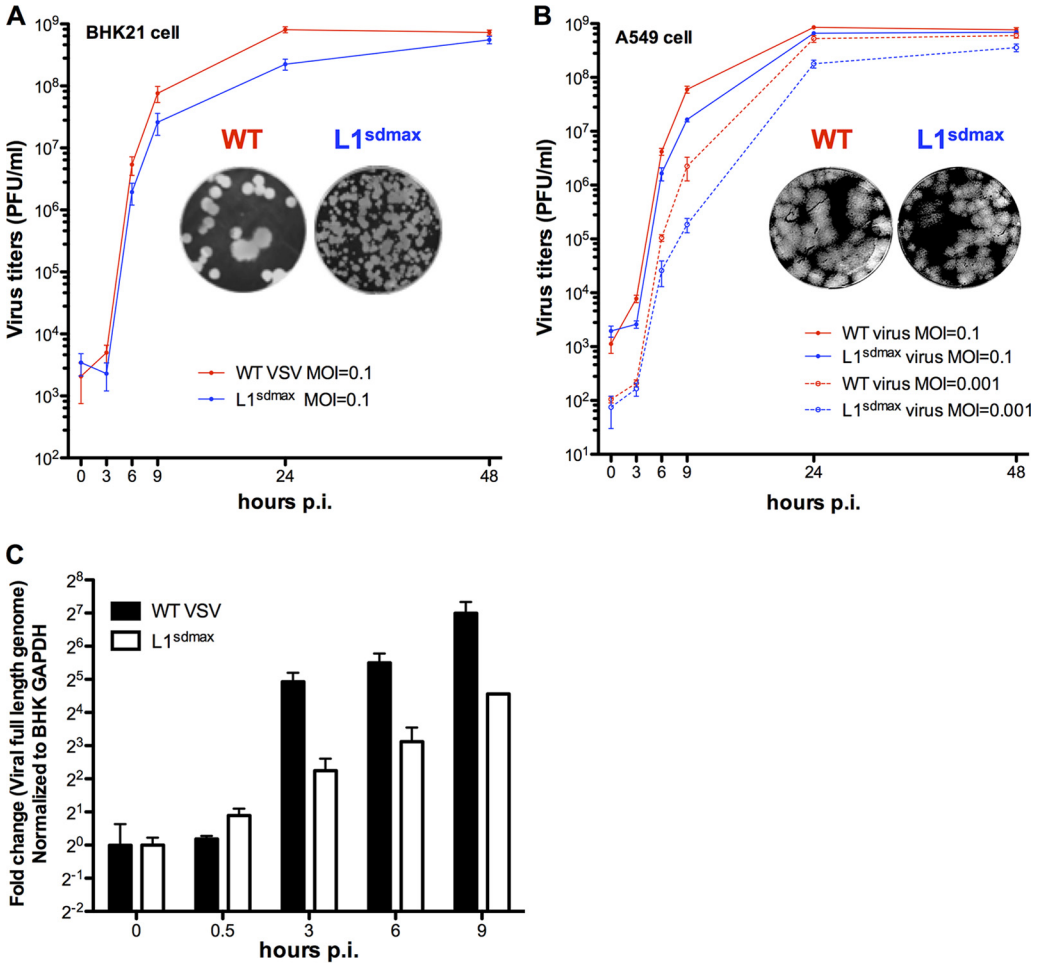


**FIG 2** Multistep growth kinetics and plaque phenotypes of WT and L1$^{sdmax}$ virus in BHK-21 cells (A) and A549 cells (B) at low MOIs. (C) Quantitative RT-PCR was conducted to quantitate the full-length viral RNA in WT- and L1$^{sdmax}$-infected BHK-21 cells (MOI = 3).

derrepresented or overrepresented codon pairs, resulting in hundreds of synonymous nucleotide substitutions (see Table S1 in the supplemental material). Compared to its WT counterpart, L1$^{min}$ has a much lower codon pair score, whereas L1$^{sdmax}$ has a significantly higher one (Fig. 1B). We took into account a possible increase in the frequency of XXCpGXX, a dinucleotide formed between two codons that may play a role in inducing an innate immune response (23), and of XXUpAXX, a dinucleotide that at high frequency has been proposed to reduce mRNA stability (24). We particularly avoided generating extra AAAUU (AU-rich) sequences, which are signals for mRNA degradation (25). The distribution of overrepresented and underrepresented codon pairs in these designs is graphed in Fig. S1 in the supplemental material.

A recombinant VSV bearing a "deoptimized" L gene (L1$^{min}$) is expected to be highly attenuated and possibly nonviable. On the other hand, based on our previous experience in "maximizing" the poliovirus P1 region, we anticipated that sdmax might not affect L gene expression negatively (17). We initially included the sdmax design in our study in order to rule out the possibility that certain unidentified RNA sequences critical for virus replication were accidentally modified during the large-scale recoding (26). As shown in Table S1, about 33% of the nucleotides of the L1 region have been mutated in the L1$^{sdmax}$ design; therefore, theoretically, any important RNA signal or highly structured element longer than 3 or 4 nucleotides (nt) would have been inactivated.

cDNAs corresponding to these recoded regions were chemically synthesized *de novo* and cloned into the parental antigenomic plasmid pVSV1(+) to replace the WT sequence. The reverse genetics of these recombinant viruses was carried out using the vaccinia virus-mediated system (27). The L1$^{sdmax}$ design yielded infectious virus after one blind passage, whereas L1$^{min}$ failed to generate a viable virus.

The growth phenotypes of the recombinant L1$^{sdmax}$ virus was then analyzed in tissue culture. Compared to the WT virus, the plaque phenotypes revealed slightly smaller sizes in BHK-21 cells and A549 cells (Fig. 2A and B). Multistep growth kinetics, analyzed in BHK-21 or A549 cells by inoculation at a low multiplicity of infection (MOI) of 0.1 or 0.001, showed maximal titers of L1$^{sdmax}$ between 24 and 48 hpi that were comparable to that of the WT virus. Viral replication of L1$^{sdmax}$, however, was slightly delayed, independent of the cell type it infected. A quantitative reverse transcription-PCR (RT-PCR) assay that measured the level of viral full-length RNA in infected BHK-21 cells supported the delay of genome synthesis (Fig. 2C). To measure the yield of viral proteins and expand the range of cell types, we then determined the synthesis of N protein by immunocytochemistry in HeLa cells.

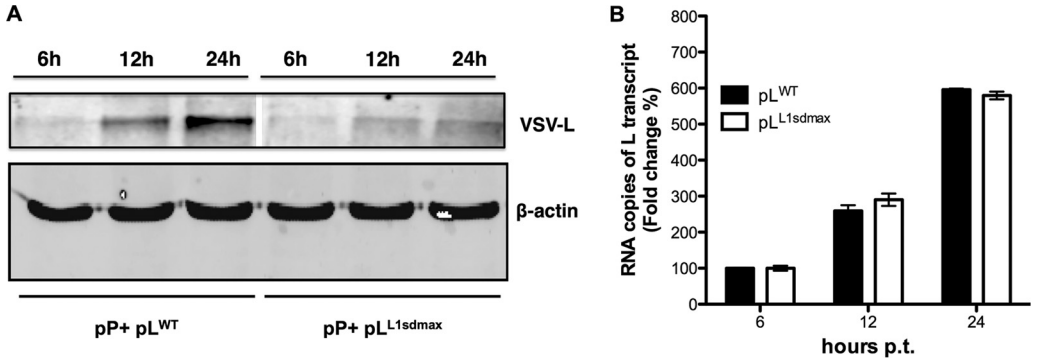


**FIG 3** The expression of L1$^{sdmax}$ sequence was examined by transfecting pL$^{L1sdmax}$ plasmid into BHK-21 cells that were previously infected with T7 polymerase (Pol)-expressing vaccinia virus vTF7-3. (A) The L protein expression in transfected cells was examined by Western blotting. (B) The synthesis of L mRNA was examined by quantitative RT-PCR (qRT-PCR). pt, posttransfection.

In L1$^{sdmax}$-infected cells, at 4 hpi, much less viral N protein was detected than in WT virus-infected cells (see Fig. S2 in the supplemental material).

**Reduced expression of the L protein encoded by the L1$^{sdmax}$ sequence.** During the early stages of virus infection, the slower growth of the L1$^{sdmax}$ virus led to a reduced yield of all the viral products (see Fig. S3 in the supplemental material). We were unable to explain the decreased level of L protein synthesis by simply comparing the yields of viral protein to those of mRNA. To circumvent this problem, we constructed two L expression plasmids (designated pL$^{L1sdmax}$ and pL$^{L1min}$) (see Fig. S4 in the supplemental material) by replacing the cognate WT L open reading frames of pL with the synthetic L derivatives (L1$^{sdmax}$ and L1$^{min}$). We then examined the production of full-length L protein after transiently transfecting BHK-21 cells that were previously infected with vTF7-3. In this experimental setting, the entire L gene coding sequences are transcribed in the cytoplasm by T7 polymerase.

To increase the stability of the large polymerase polypeptide, we cotransfected into BHK-21 cells a plasmid expressing the VSV P protein together with the plasmid harboring the modified L sequence (28). In comparison to translation of pL$^{WT}$, translation of the L1$^{sdmax}$ gene produced only a weak signal (Fig. 3A), even though equal amounts of L transcripts were detected in pL$^{WT}$- and pL$^{L1sdmax}$-transfected cells (Fig. 3B). This result was unexpected given that codon pairing in L1$^{sdmax}$ has been designed to yield mRNA favorable for translation (17). The synthesis of L1$^{min}$ was even more inefficient than that of L1$^{sdmax}$ (see Fig. S4B in the supplemental material). This was not totally unexpected, although we do not know as yet whether the poor L1$^{min}$ synthesis is due to an inhibition of translation *per se* or a rapid degradation of mRNA prior to or during translation.

Another interesting observation is that the L1$^{sdmax}$ virus showed an exquisite sensitivity to the pharmaceutical deprivation of Hsp90 (see Fig. S5 in the supplemental material), a host chaperone molecule that has been identified to be essential for the proper folding of the newly synthesized VSV L protein (29). It raises the possibility that an enhanced chaperone engagement may be required for the L1$^{sdmax}$ virus.

**Diminished virulence of the L1$^{sdmax}$ virus after intranasal inoculation of mice.** As mentioned above, the poliovirus variant P1$^{max}$ in which the capsid coding region was codon pair optimized, was as lethal in CD155 transgenic mice as WT poliovirus (17). We therefore tested the pathogenesis of L1$^{sdmax}$ virus in a mouse model. Five- to six-week-old male BALB/c mice were infected with different doses of WT or L1$^{sdmax}$ viruses intranasally. WT-infected mice lost weight rapidly and exhibited typical symptoms of infection starting around 3 dpi. Under our experimental conditions, the 50% lethal dose ($LD_{50}$) for WT VSV was $10^5$ PFU for intranasal infection. In contrast, neither mortality nor severe morbidity was observed in any mice infected with the L1$^{sdmax}$ virus, even at a very high infection titer ($2 \times 10^8$ PFU) (see Fig. S6B in the supplemental material). Taking these data together, we conclude that L1$^{sdmax}$ virus is highly attenuated in BALB/c mice. This was a surprise, but it matched our unpublished results obtained with recoded dengue virus variants that phenotypes observed in tissue culture with a codon pair-recoded virus do not necessarily predict phenotypes of the same recoded virus when it is tested in experimental animals.

**Virus burdens in the infected organs.** The efficacy of live attenuated vaccines depends on reduced viral replication *in vivo* but a successful stimulation of immunological memory (18). Moreover, virulence and virus load in infected organs are usually positively correlated (19). Therefore, we examined virus burden in the infected animals by both plaque-forming assays and quantitative RT-PCR. At 3 dpi, the virus load in the L1$^{sdmax}$-infected organs was at least two orders of magnitude less than that in their WT-infected counterparts. On day 6, the infectious L1$^{sdmax}$ virus could not be recovered in any of the mice lungs that we examined and could be detected in only one brain sample ($n = 3$) (Fig. 4A). In contrast, in WT-virus-infected animals, a virus burden of approximate $10^4$ PFU/g was observed in brain tissues up to 6 dpi, which ultimately resulted in the death of all the remaining animals by 9 dpi (data not shown). We also examined the viral RNA load in mouse brains using quantitative RT-PCR (Fig. 4B). Total RNA was extracted from infected brains, and a 150-bp fragment corresponding to the viral N gene was amplified. Viral RNA was present in every brain of the infected animals, but the viral RNA load of L1$^{sdmax}$-infected animals was lower than that of WT virus-infected ones.

**Disparate histopathology of WT- and L1$^{sdmax}$-infected brains.** Even the limited replication of L1$^{sdmax}$ in the brains of infected animals raises the question of whether such viral variants could serve as vaccine candidates. We therefore carried out histological studies. BALB/c mice were infected intranasally with $10^7$ PFU of viruses, and brains were harvested for hematoxylin-and-eosin (H&E) staining after 5 days. Brain tissues infected with

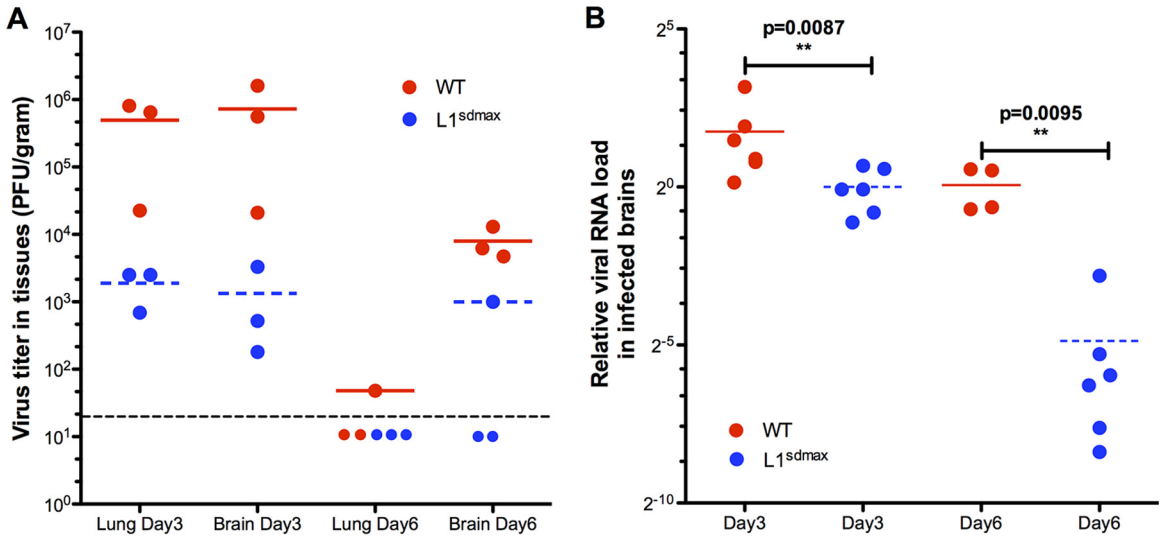


**FIG 4** Attenuation of L1$^{sdmax}$ VSV in mice. (A) BALB/c mice were infected with WT or L1$^{sdmax}$, and viral loads in organs were determined by plaque assay. At 6 dpi, the infectious viruses were undetectable in all but one WT-infected lung, and the presence of infectious virus could be detected in only one L1$^{sdmax}$-infected brain ($n = 3$). The dashed line indicates the limit of detection (30 PFU/g) for plaque assay. (B) The viral RNA loads in mice brains were measured using quantitative RT-PCR (**, $P < 0.01$ [two-tailed Mann-Whitney U test]).

WT VSV exhibited severe immunopathological characteristics, evidenced by multifocal perivascular cuffing, mononuclear cell infiltration in the parenchyma, meningeal mononuclear cell infiltration, and hemorrhage (Fig. 5), consistent with previous studies (14, 30). Tissues collected from the L1$^{sdmax}$ group exhibit only mild, if any, inflammatory changes upon virus infection.

VSV infection compromises the integrity of the blood-brain barrier (BBB) (31). The destruction of BBB accompanied by the intensive immunological infiltration causes severe immunopathogenesis that leads directly to the death of experimental animals. Therefore, we used the well-established Evans blue assay to assess the integrity of the BBB after virus infection, a method providing an additional indicator of virus pathogenesis (32). As shown in Fig. S6C in the supplemental material, at 6 dpi the brain of the animal infected with L1$^{sdmax}$ showed no sign of BBB damage, whereas a widespread, intensive parenchyma staining was apparent in the WT-infected brain, which is a clear sign of diminished BBB integrity.

**The immune response in L1$^{sdmax}$-infected mice.** We next determined whether the restricted replication of this viral variant provides effective immunological protection against challenge with WT virus. We vaccinated 5- to 6-week-old BALB/c mice with different doses of L1$^{sdmax}$ virus intranasally. After 3 weeks, all mice received $10^7$ PFU of WT virus intranasally, representing an approximately 100-fold $LD_{50}$ of WT VSV. None of the L1$^{sdmax}$-immunized mice exhibited signs of disease, and their body weights increased steadily, whereas age-matched naive mice succumbed to challenge after 6 to 8 days (Fig. 6A).

We then asked whether the L1$^{sdmax}$ immunization elicited a B cell-mediated humoral immunity. Sera were collected 21 days postvaccination from tail vein blood, and titers of virus-specific neutralizing antibodies (NAb) were measured. The L1$^{sdmax}$ virus was capable of inducing a robust protective antibody response (Fig. 6B). A similar level of NAb was detected in mice that were immunized with the same amount of WT or L1$^{sdmax}$ virus, whereas the control group did not develop a detectable humoral response against VSV infection. Taken together, these data indicate that a single-dose vaccination of the L1$^{sdmax}$ virus can elicit a potent immune response that fully protects mice from a subsequent virulent challenge.

**Prolonged induction of proinflammatory cytokines and chemokines in WT- but not in L1$^{sdmax}$-infected brains.** During VSV infection, mouse susceptibility correlated positively with extensive cytokine/chemokine expression in the central nervous system (CNS) (14). To determine the nature of the inflammatory response during L1$^{sdmax}$ infection, we profiled the transcription levels of several proinflammatory cytokines and chemokines in virus-infected brains. Compared to their WT-infected counterparts, MCP-1 and RANTES were induced to a lesser extent in L1$^{sdmax}$-infected mice (Fig. 7A). Additionally, at 3 dpi, L1$^{sdmax}$-infected mice showed levels of tumor necrosis factor alpha (TNF-$\alpha$) and interleukin 6 (IL-6) similar to those of WT-infected animals (Fig. 7B). WT-infected mice retained a high level of cytokine production until 6 dpi, while L1$^{sdmax}$-infected mice showed a significant decline of cytokine synthesis by then. This suggests that in contrast to the highly attenuated L1$^{sdmax}$ virus, WT virus infection in the CNS cannot be controlled without a sustained inflammation, which eventually leads to immunopathogenesis and irreversible neuron damage.

## DISCUSSION

**Impact of codon pair deoptimization on gene expression.** In this study, we evaluated the consequences of large-scale L gene recoding upon VSV replication and pathogenesis. The L1 region comprises the coding sequences of domains I to III and part of domain IV, which primarily forms the core ring structure of the VSV RNA-dependent RNA polymerase (RdRp) and catalyzes RNA polymerization (33). The L1$^{min}$ sequence yielded only trace amounts of full-length L protein after transient expression in tissue culture cells, which is reminiscent of data obtained with variants of codon pair-deoptimized poliovirus and influenza virus (17–19).

Codon pair deoptimization appears to affect several mecha-

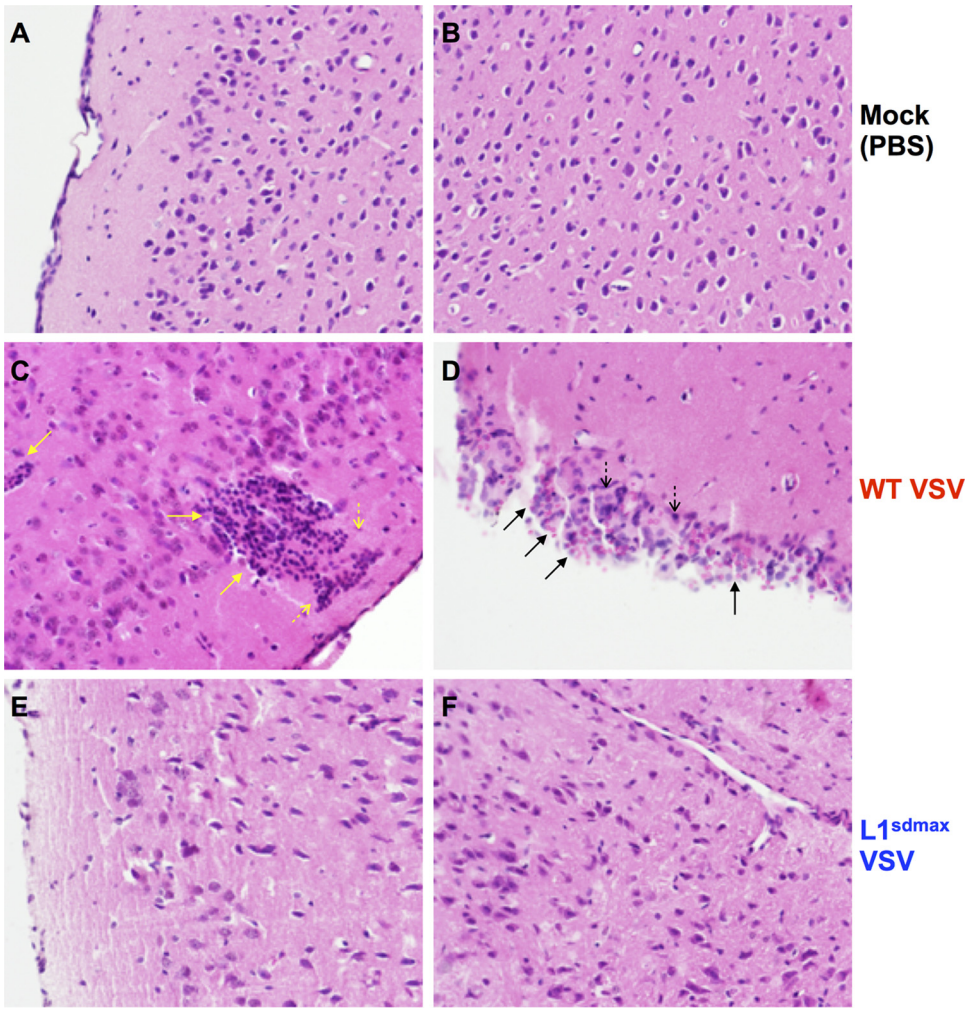


**FIG 5** Histopathology after VSV infection. Mice were inoculated with PBS (A and B), $10^7$ PFU WT (C and D), or $L1^{sdmax}$ (E and F) virus intranasally, and the horizontal brain sections containing cerebral cortex were stained with H&E at 5 dpi. Representative brain histology is shown for each group (magnification, ×40). In panel C, solid yellow arrows indicate the perivascular cuffing, and dashed yellow arrows indicate the mononuclear cell infiltration in the brain parenchyma. In panel D, solid black arrows indicate meningeal hemorrhage, and dashed black arrows indicate the meningeal mononuclear cell infiltration.

nisms that interfere with gene expression in a context-dependent manner. For example, it might be difficult for the ribosome to read through a string of "rare" codon pairs, a predicament leading to less protein production per mRNA. In addition, it is known that the dinucleotide frequency of CpG and UpA in eukaryotic RNA viruses, as well as in mammalian mRNA in general, is lower than expected (34–36), a phenomenon that must be advantageous for viruses. Generating rare codon pairs by rearranging existing synonymous codons inadvertently leads to an enrichment of UpA and CpG dinucleotides in the mRNA sequences. For instance, the $L1^{min}$ but not the $L1^{sdmax}$ design contains significantly more XXUpAXX and XXCpGXX dinucleotides than the WT sequence (see Table S1 in the supplemental material), with the increase mapping to between codons, as shown, since codon use remained unchanged. Recent studies suggest that the dinucleotide composition in RNA virus genomes influences RNA virus replication, possibly because of an unclear host-pathogen interaction (37) and/or increased instability of the mRNA (23). Although we cannot exclude the possibility that strengthened host recognition of UpA/CpG dinucleotides contributed to the attenuation phenotype of our codon pair-deoptimized viruses, the reverse genetics of $L1^{min}$ was conducted in BHK-21 cells, a cell line well known for its deficiency in innate immune response (38). Hence, the nonviable phenotype of the $L1^{min}$ design cannot be simply attributed to an enhanced host response.

**Impact of codon pair "scramble-max" on protein synthesis.** The most striking phenotype that we observed with $L1^{sdmax}$ is its attenuation that results from an enrichment of overrepresented codon pairs. Our previous experiments in which we "maximized" the encoding of the poliovirus P1 region suggested that such genetic alteration enhanced the expression of the corresponding viral ORF without affecting virulence (17). This appears to be contrary to the observation in this study. The attenuation of $L1^{sdmax}$ is not host range restricted, because the virus forms smaller plaques in all cell lines tested. Considering that the transcriptional regulatory sequences in the untranslated region of the L gene were never altered, it becomes less likely that the $L1^{sdmax}$ sequence is inadequately transcribed by the viral polymerase. Indeed, the poor expression of the $L1^{sdmax}$ sequence does not seem to occur at the transcription level, because (i) a high level of L mRNA was de-

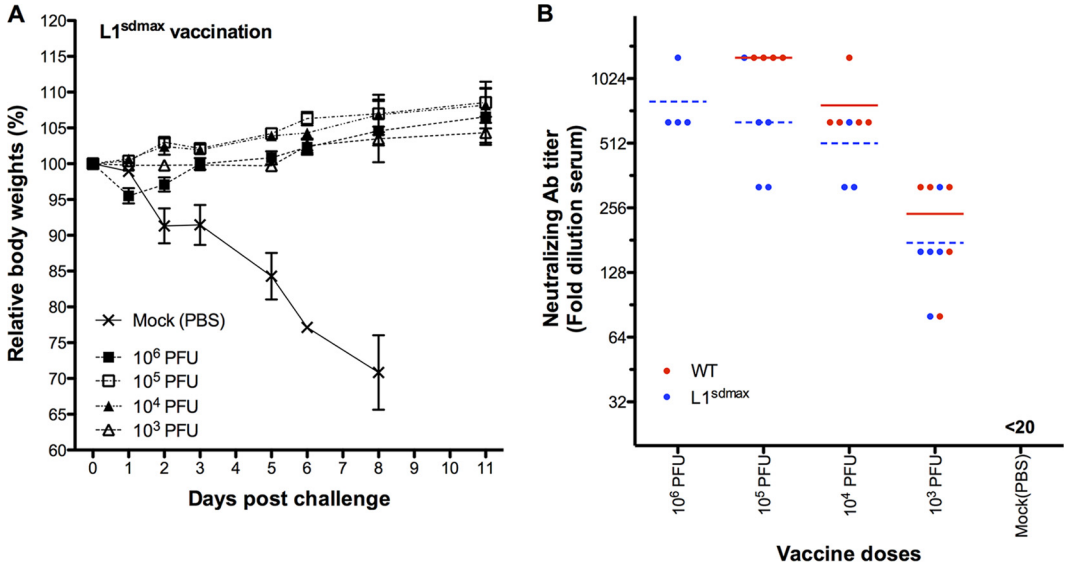


**FIG 6** Immunogenicity of the L1$^{sdmax}$ virus. (A) Dynamics of L1$^{sdmax}$-immunized mice body weights after a lethal WT challenge at day 21. (B) Titers of virus-specific neutralizing antibody (NAb) in WT- and L1$^{sdmax}$-immunized mice 21 days after the primary exposure. For this experiment, *n* was 5 per group. A larger number of animals ($n = 10$) for the groups infected with $10^5$ PFU of the WT were initially immunized, because the infection titer is close to the $LD_{50}$ of WT virus. The sera from the survivors (4/10) were subsequently collected at 21 dpi, and the titers of virus-specific neutralizing antibody were determined as described in Materials and Methods.

tected when the L1$^{sdmax}$ sequence was placed under the control of the T7 promoter and transfected into cells expressing T7 polymerase (Fig. 3B) and (ii) during L1$^{sdmax}$ virus infection, the same kinetics of mRNA accumulation were found for the L and N genes (see Fig. S3 in the supplemental material) (ranging from 1 hpi to 6 hpi).

Considering the possibility that an enhanced chaperone engagement might be required for the L1$^{sdmax}$ virus (see Fig. S5 in the supplemental material), we hypothesized that the alteration of the translation elongation rate, presumably caused by the accumulation of overrepresented codon pairs, might interfere with the coordination between translation and other events closely related to translation rate, such as protein folding. Recent reports have shown that clustered rare codons are frequently distributed between defined protein domains, especially for large multidomain proteins. This distribution pattern of "slow" codons might collectively reduce the read-through activity of the ribosome, which turns out to be beneficial for proper protein folding (39, 40). An early study conducted in a bacterial system also suggests that codon pair utilization influences protein folding by altering translational efficiency, although only a small number of codon pairs was included and analyzed at that time (41). Herein we speculate that the folding efficiency of a multidomain protein, like the VSV L protein described in this paper, might be perturbed by the large-scale genome recoding. The relatively low codon pair bias in the WT L1 region (Fig. 1B) might be a compromise between translation accuracy and folding efficiency.

**L1$^{sdmax}$ serves as a candidate for VSV-based vaccines and vectors.** VSV has been studied as an agent with unique oncolytic properties aided by its broad tissue tropism and exquisite sensitivity to innate immunity, which result in its preferential replication in tumors. In addition, VSV might serve as an excellent vaccine delivery platform, because of its easily manipulated genome and the capacity to stimulate a robust cytokine response via mucosal delivery. In this study, we generated and identified a recombinant virus, L1$^{sdmax}$, which is highly attenuated (its $LD_{50}$ is at least 2,000-fold more than that of the WT). Our results showed that L1$^{sdmax}$ underwent a limited replication and dissemination *in vivo* that barely caused any morbidity, but this self-restricted infection was highly immunogenic. The L1$^{sdmax}$ virus appears to be an attractive live vaccine candidate applicable to other viruses in the order of *Mononegavirales* that encode very large polymerase polypeptides. In the development of vaccines, conventional strategies usually lead to a limited number of mutations in viral genomes, whereas L1$^{sdmax}$ carries in its L-encoding segment 858 point mutations. We have passaged the L1$^{sdmax}$ virus 5 times in BHK-21 cells at low MOIs, and we did not observe any phenotypic reversion (data not shown), but long-term passaging is required to confirm genetic stability. Of course, the current construct may have to be further attenuated to avoid all proliferation in the CNS.

The recent Ebola outbreak in West Africa and the sporadic cases in the Western Hemisphere have elicited international concern. One of the most promising vaccine candidates against Ebola infection, VSV-ZEBOV, is a VSV chimera that expresses Ebola genetic information (42). It will be of interest to further evaluate the safety and efficacy of L1$^{sdmax}$ as a platform to deliver foreign antigens.

In summary, the present study describes the first large-scale recoding of VSV, a rhabdovirus that belongs to a large family of human pathogens. The outcome of the experiments is surprising but nevertheless may herald a unique approach to develop live attenuated strains for VSV and possibly other NNS viruses.

## MATERIALS AND METHODS

**Cells and viruses.** BHK-21, Vero, A549, and HeLa cells were maintained in Dulbecco's modified Eagle medium (DMEM) plus 10% fetal bovine serum at 37°C. WT VSV is recovered from the cDNA clone pVSV1(+), using the well-established vaccinia virus-mediated system (27). Briefly, to

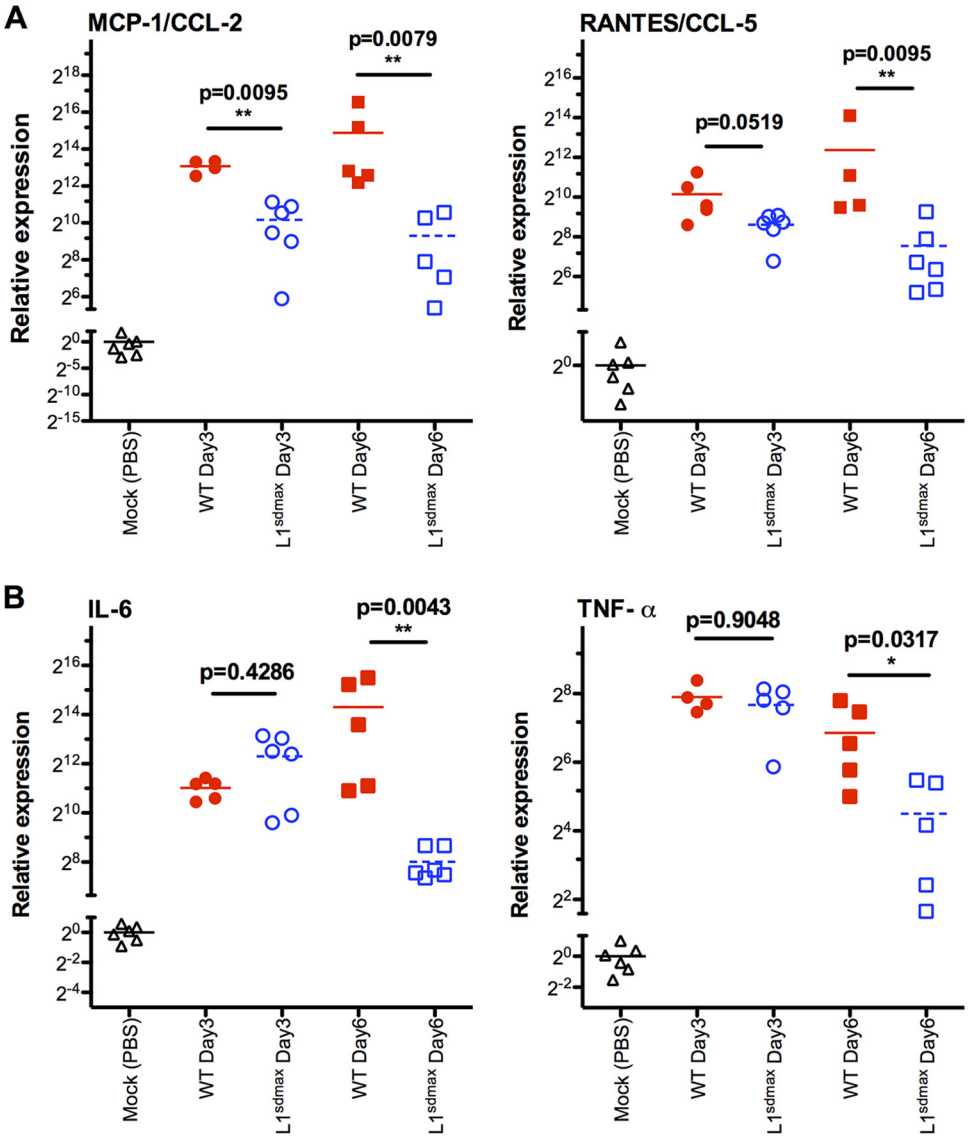


**FIG 7** Cytokine/chemokine profile after virus infection. (A) Quantitative RT-PCR to measure chemokine (MCP-1 and RANTES) expression relative to the mouse β-actin after virus infection. (B) Proinflammatory cytokine induction in PBS-, WT-, and L1$^{sdmax}$-inoculated mice. Data were collected from 4 to 6 mice per group. Statistical significance is indicated by asterisks (*, $P < 0.05$; **, $P < 0.01$ [two-tailed Mann-Whitney U test]).

construct the cDNA clone of L1$^{sdmax}$ or L1$^{min}$ virus, the HpaI-to-AvaI fragment of pVSV1(+) was replaced with the corresponding synthetic fragment L1$^{sdmax}$ or L1$^{min}$ (GenScript, NJ, USA) in which overrepresented or underrepresented codon pairs were substantially enriched. The recovered viruses were plaque purified, and their full-length sequences were confirmed by RT-PCR.

**Virus load and protection assay.** Animal studies were carried out in accordance with a protocol that adhered to the *Guide for the Care and Use of Laboratory Animals* of the NIH (43) and was reviewed and approved (approval number 354543) by the Stony Brook University Institutional Animal Care and Use Committee (IACUC). Five- to six-week-old male BALB/c mice (Taconic Farms, Inc.) were intranasally infected with $5 \times 10^6$ PFU viruses, and at 3 and 6 dpi, their lungs and brains were harvested for determinations of virus titers by plaque-forming assay. For viral RNA load analysis, total RNA was extracted from brains of mice (TRIzol; Life Technologies) that were infected with $5 \times 10^6$ PFU viruses, and the abundance of viral RNA was subsequently evaluated by real-time RT-PCR using a primer pair that recognizes the viral N gene (VSV N primer) (see Table S2 in the supplemental material). In parallel, qPCR directed against mouse β-actin mRNA was performed to control for any differences in the amount of total RNA inputs (mouse β-actin primer) (Table S2 in the supplemental material). For protection assay, mice were vaccinated intranasally with various doses of L1$^{sdmax}$ virus and challenged with $10^7$ PFU of WT virus at 21 days after vaccination. A group of age-matched virus-naive mice ($n = 3$) were challenged as well, as a negative control. After the virulent challenge, the mice body weights and neuronal disorder symptoms were closely monitored for another 14 days.

**Neutralizing antibody assay.** The mice were immunized with various doses of either WT or L1$^{sdmax}$ virus intranasally. The serum was isolated from tail vein blood 21 days after vaccination, followed by a 2-fold serial dilution in DMEM starting at a dilution of 1:20. Fifty microliters of the diluted serum was incubated with 100 PFU WT VSV in 50 μl DMEM at 37°C for 1 h. One hundred microliters of Vero cell suspension was then combined with the mixture and seeded on 96-well plates in triplicate. Cell morphology was checked daily, and after a 48-h incubation at 37°C, the remaining cells were stained with 1% crystal violet. The reciprocal of the

dilution that gives 100% protection from VSV CPE was recorded as the virus-specific neutralizing-antibody titer.

**Histopathology.** Mice were infected with $10^7$ PFU virus by intranasal inoculation and euthanized at 5 dpi. Mice were transcardially perfused with 10% paraformaldehyde (PFA)-phosphate-buffered saline (PBS) and their brains were harvested and fixed in 10% PFA-PBS, followed by 50% ethanol processing and paraffin embedding. The brain tissues were subsequently sectioned at 5 $\mu$m and stained with H&E. The histopathological results were examined independently by two neuropathologists at the School of Medicine, Stony Brook University.

**Quantitative RT-PCR to analyze cytokine/chemokine inductions.** Total RNA was extracted from mice brains inoculated with PBS, WT, or $L1^{sdmax}$ at both 3 and 6 dpi and then treated with RNase-free DNase I (Life Technologies) for 30 min at 37°C before a reverse transcription was conducted with oligo$(dT)_{20}$ (SuperScript III; Life Technologies). Quantitative PCR was subsequently performed to evaluate the induction of cytokines and chemokines using gene-specific primers (see Table S2 in the supplemental material). All reactions were subsequently normalized to the RNA levels of mouse $\beta$-actin and reported as increases in induction over that in PBS-inoculated animals.

**Quantitative RT-PCR to measure viral genome replication.** BHK-21 cells were infected with viruses at a MOI of 3. At various time points, total RNA was extracted and reverse transcribed by random hexamer priming. Quantitative PCR was carried out with a primer pair spanning the region between the VSV G and L genes (see Table S2 in the supplemental material) to measure the viral genome replication. The reaction results were normalized to the mRNA levels of the BHK-21 GAPDH gene and reported as the increase (fold) over the value at 0 hpi.

**Plasmid construction and transient protein expression.** The corresponding region of the WT L gene in the expression plasmid pL (27) was replaced by two recoded derivatives using the XhoI and XbaI digestion sites. For transient expression, $10^6$ BHK-21 cells were infected with vTF7-3 for 1 h and then cotransfected with 1.5 $\mu$g pP and 1.25 $\mu$g pL derivatives. Whole-cell lysates and total RNA were harvested at various time points, and the yield of viral products was subsequently determined by Western blotting and quantitative RT-PCR.

**Statistical analysis.** Statistical analysis was performed using GraphPad Prism software version 5.0c (San Diego, CA). Data are presented as means with standard deviations (SDs). Two-tailed Mann-Whitney U tests were used for Fig. 4B and 7.

## SUPPLEMENTAL MATERIAL

Supplemental material for this article may be found at http://mbio.asm.org/lookup/suppl/doi:10.1128/mBio.00237-15/-/DCSupplemental.

Figure S1, TIF file, 2 MB.
Figure S2, TIF file, 1.7 MB.
Figure S3, TIF file, 0.5 MB.
Figure S4, TIF file, 0.6 MB.
Figure S5, TIF file, 0.4 MB.
Figure S6, TIF file, 1.8 MB.
Table S1, TIF file, 0.5 MB.
Table S2, TIF file, 0.7 MB.

## ACKNOWLEDGMENTS

We greatly appreciate Yutong Song and Yu Sun for their kind help with plasmid construction and H&E staining, Jingxuan Liu and James Davis for their efforts in providing expert opinions for the histopathological studies, and Jeronimo Cello and Astrid Wimmer for a critical reading of the manuscript.

This work was supported in part by NIH grant R01 AI075219 to E.W. and NIH grant R01 AI059371 to S.P.J.W.

## REFERENCES

1. **White JM, Schornberg KL**. 2012. A new player in the puzzle of filovirus entry. Nat Rev Microbiol **10:**317–322. http://dx.doi.org/10.1038/nrmicro2764.
2. **Eaton BT, Broder CC, Middleton D, Wang LF**. 2006. Hendra and Nipah viruses: different and dangerous. Nat Rev Microbiol **4:**23–35. http://dx.doi.org/10.1038/nrmicro1323.
3. **Collins PL, Melero JA**. 2011. Progress in understanding and controlling respiratory syncytial virus: still crazy after all these years. Virus Res **162:**80–99. http://dx.doi.org/10.1016/j.virusres.2011.09.020.
4. **Lichty BD, Power AT, Stojdl DF, Bell JC**. 2004. Vesicular stomatitis virus: re-inventing the bullet. Trends Mol Med **10:**210–216. http://dx.doi.org/10.1016/j.molmed.2004.03.003.
5. **Quiroz E, Moreno N, Peralta PH, Tesh RB**. 1988. A human case of encephalitis associated with vesicular stomatitis virus (Indiana serotype) infection. Am J Trop Med Hyg **39:**312–314.
6. **Brown F, Bishop DH, Crick J, Francki RI, Holland JJ, Hull R, Johnson K, Martelli G, Murphy FA, Obijeski JF, Peters D, Pringle CR, Reichmann ME, Schneider LG, Shope RE, Simpson DI, Summers DF, Wagner RR**. 1979. Rhabdoviridae. Report of the Rhabdovirus Study Group, International Committee on Taxonomy of Viruses. Intervirology **12:**1–7. http://dx.doi.org/10.1159/000149062.
7. **Das K, Aramini JM, Ma LC, Krug RM, Arnold E**. 2010. Structures of influenza A proteins and insights into antiviral drug targets. Nat Struct Mol Biol **17:**530–538. http://dx.doi.org/10.1038/nsmb.1779.
8. **Sleat DE, Banerjee AK**. 1993. Transcriptional activity and mutational analysis of recombinant vesicular stomatitis virus RNA polymerase. J Virol **67:**1334–1339.
9. **Li J, Fontaine-Rodriguez EC, Whelan SP**. 2005. Amino acid residues within conserved domain VI of the vesicular stomatitis virus large polymerase protein essential for mRNA cap methyltransferase activity. J Virol **79:**13373–13384. http://dx.doi.org/10.1128/JVI.79.21.13373-13384.2005.
10. **Li J, Rahmeh A, Morelli M, Whelan SP**. 2008. A conserved motif in region V of the large polymerase proteins of nonsegmented negative-sense RNA viruses that is essential for mRNA capping. J Virol **82:**775–784. http://dx.doi.org/10.1128/JVI.02107-07.
11. **Rahmeh AA, Li J, Kranzusch PJ, Whelan SP**. 2009. Ribose 2′-O methylation of the vesicular stomatitis virus mRNA cap precedes and facilitates subsequent guanine-N-7 methylation by the large polymerase protein. J Virol **83:**11043–11050. http://dx.doi.org/10.1128/JVI.01426-09.
12. **Poch O, Blumberg BM, Bougueleret L, Tordo N**. 1990. Sequence comparison of five polymerases (L proteins) of unsegmented negative-strand RNA viruses: theoretical assignment of functional domains. J Gen Virol **71:**1153–1162. http://dx.doi.org/10.1099/0022-1317-71-5-1153.
13. **Johnson JE, Nasar F, Coleman JW, Price RE, Javadian A, DraperK, Lee M, Reilly PA, Clarke DK, Hendry RM, Udem SA**. 2007. Neurovirulence properties of recombinant vesicular stomatitis virus vectors in nonhuman primates. Virology **360:**36–49. http://dx.doi.org/10.1016/j.virol.2006.10.026.
14. **Hou YJ, Banerjee R, Thomas B, Nathan C, García-Sastre A, Ding A, Uccellini MB**. 2013. SARM is required for neuronal injury and cytokine production in response to central nervous system viral infection. J Immunol **191:**875–883. http://dx.doi.org/10.4049/jimmunol.1300374.
15. **Gutman GA, Hatfield GW**. 1989. Nonrandom utilization of codon pairs in *Escherichia coli*. Proc Natl Acad Sci U S A **86:**3699–3703. http://dx.doi.org/10.1073/pnas.86.10.3699.
16. **Hatfield GW, Gutman GA**. 1993. Codon pair utilization bias in bacteria, yeast and mammals, p 164–171. *In* Hatfield D, Lee BJ, Pirtle RM (ed), Transfer RNA in protein synthesis. CRC Press, Boca Raton, FL.
17. **Coleman JR, Papamichail D, Skiena S, Futcher B, Wimmer E, Mueller S**. 2008. Virus attenuation by genome-scale changes in codon pair bias. Science **320:**1784–1787. http://dx.doi.org/10.1126/science.1155761.
18. **Mueller S, Coleman JR, Papamichail D, Ward CB, Nimnual A, Futcher B, Skiena S, Wimmer E**. 2010. Live attenuated influenza virus vaccines by computer-aided rational design. Nat Biotechnol **28:**723–726. http://dx.doi.org/10.1038/nbt.1636.
19. **Yang C, Skiena S, Futcher B, Mueller S, Wimmer E**. 2013. Deliberate reduction of hemagglutinin and neuraminidase expression of influenza virus leads to an ultraprotective live vaccine in mice. Proc Natl Acad Sci U S A **110:**9481–9486. http://dx.doi.org/10.1073/pnas.1307473110.
20. **Le Nouën C, Brock LG, Luongo C, McCarty T, Yang L, Mehedi M, Wimmer E, Mueller S, Collins PL, Buchholz UJ, DiNapoli JM**. 2014. Attenuation of human respiratory syncytial virus by genome-scale codon-pair deoptimization. Proc Natl Acad Sci U S A **111:**13169–13174. http://dx.doi.org/10.1073/pnas.1411290111.
21. **Mueller S, Coleman JR, Wimmer E**. 2009. Putting synthesis into biology: a viral view of genetic engineering through de novo gene and genome

synthesis. Chem Biol **16:**337–347. http://dx.doi.org/10.1016/j.chembiol.2009.03.002.
22. **Combe M, Sanjuán R.** 2014. Variation in RNA virus mutation rates across host cells. PLopS Pathog **10:**e1003855. http://dx.doi.org/10.1371/journal.ppat.1003855.
23. **Burns CC, Campagnoli R, Shaw J, Vincent A, Jorba J, Kew O.** 2009. Genetic inactivation of poliovirus infectivity by increasing the frequencies of CpG and UpA dinucleotides within and across synonymous capsid region codons. J Virol **83:**9957–9969. http://dx.doi.org/10.1128/JVI.00508-09.
24. **Al-Saif M, Khabar KS.** 2012. UU/UA dinucleotide frequency reduction in coding regions results in increased mRNA stability and protein expression. Mol Ther **20:**954–959. http://dx.doi.org/10.1038/mt.2012.29.
25. **Chen CY, Shyu AB,** 1995. AU-rich elements: characterization and importance in mRNA degradation. Trends Biochem Sci **20:**465–470.
26. **Song Y, Liu Y, Ward CB, Mueller S, Futcher B, Skiena S, Paul AV, Wimmer E.** 2012. Identification of two functionally redundant RNA elements in the coding sequence of poliovirus using computer-generated design. Proc Natl Acad Sci U S A **109:**14301–14307. http://dx.doi.org/10.1073/pnas.1211484109.
27. **Whelan SP, Ball LA, Barr JN, Wertz GT.** 1995. Efficient recovery of infectious vesicular stomatitis virus entirely from cDNA clones. Proc Natl Acad Sci U S A **92:**8388–8392. http://dx.doi.org/10.1073/pnas.92.18.8388.
28. **Canter DM, Perrault J.** 1996. Stabilization of vesicular stomatitis virus L polymerase protein by P protein binding: a small deletion in the C-terminal domain of L abrogates binding. Virology **219:**376–386. http://dx.doi.org/10.1006/viro.1996.0263.
29. **Connor JH, McKenzie MO, Parks GD, Lyles DS.** 2007. Antiviral activity and RNA polymerase degradation following Hsp90 inhibition in a range of negative strand viruses. Virology **362:**109–119. http://dx.doi.org/10.1016/j.virol.2006.12.026.
30. **Ma Y, Wei Y, Zhang X, Zhang Y, Cai H, Zhu Y, Shilo K, Oglesbee M, Krakowka S, Whelan SP, Li J.** 2014. mRNA cap methylation influences pathogenesis of vesicular stomatitis virus in vivo. J Virol **88:**2913–2926. http://dx.doi.org/10.1128/JVI.03420-13.
31. **Ozduman K, Wollmann G, Piepmeier JM, van den Pol AN.** 2008. Systemic vesicular stomatitis virus selectively destroys multifocal glioma and metastatic carcinoma in brain. J Neurosci **28:**1882–1893. http://dx.doi.org/10.1523/JNEUROSCI.4905-07.2008.
32. **Bi Z, Barna M, Komatsu T, Reiss CS.** 1995. Vesicular stomatitis virus infection of the central nervous system activates both innate and acquired immunity. J Virol **69:**6466–6472.
33. **Rahmeh AA, Schenk AD, Danek EI, Kranzusch PJ, Liang B, Walz T, Whelan SP.** 2010. Molecular architecture of the vesicular stomatitis virus RNA polymerase. Proc Natl Acad Sci U S A **107:**20075–20080. http://dx.doi.org/10.1073/pnas.1013559107.
34. **Alff-Steinberger C.** 1987. Codon usage in Homo sapiens: evidence for a coding pattern on the non-coding strand and evolutionary implications of dinucleotide discrimination. J Theor Biol **124:**89–95. http://dx.doi.org/10.1016/S0022-5193(87)80254-0.
35. **Rima BK, McFerran NV.** 1997. Dinucleotide and stop codon frequencies in single-stranded RNA viruses. J Gen Virol **78:**2859–2870.
36. **Rothberg PG, Wimmer E.** 1981. Mononucleotide and dinucleotide frequencies, and codon usage in poliovirion RNA. Nucleic Acids Res **9:**6221–6229. http://dx.doi.org/10.1093/nar/9.23.6221.
37. **Atkinson NJ, Witteveldt J, Evans DJ, Simmonds P.** 2014. The influence of CpG and UpA dinucleotide frequencies on RNA virus replication and characterization of the innate cellular pathways underlying virus attenuation and enhanced replication. Nucleic Acids Res **42:**4527–4545. http://dx.doi.org/10.1093/nar/gku075.
38. **Liu WJ, Wang XJ, Clark DC, Lobigs M, Hall RA, Khromykh AA.** 2006. A single amino acid substitution in the West Nile virus nonstructural protein NS2A disables its ability to inhibit alpha/beta interferon induction and attenuates virus virulence in mice. J Virol **80:**2396–2404. http://dx.doi.org/10.1128/JVI.80.5.2396-2404.2006.
39. **Zhang G, Hubalewska M, Ignatova Z.** 2009. Transient ribosomal attenuation coordinates protein synthesis and co-translational folding. Nat Struct Mol Biol **16:**274–280. http://dx.doi.org/10.1038/nsmb.1554.
40. **Pechmann S, Frydman J.** 2013. Evolutionary conservation of codon optimality reveals hidden signatures of cotranslational folding. Nat Struct Mol Biol **20:**237–243. http://dx.doi.org/10.1038/nsmb.2466.
41. **Irwin B, Heck JD, Hatfield GW.** 1995. Codon pair utilization biases influence translational elongation step times. J Biol Chem **270:**22801–22806. http://dx.doi.org/10.1074/jbc.270.39.22801.
42. **Jones SM, Feldmann H, Ströher U, Geisbert JB, Fernando L, Grolla A, Klenk HD, Sullivan NJ, Volchkov VE, Fritz EA, Daddario KM, Hensley LE, Jahrling PB, Geisbert TW.** 2005. Live attenuated recombinant vaccine protects nonhuman primates against Ebola and Marburg viruses. Nat Med **11:**786–790. http://dx.doi.org/10.1038/nm1258.
43. **National Research Council.** 2011. Guide for the care and use of laboratory animals, 8th ed. National Academies Press, Washington, DC.